Probing Individual Steps of Dynamic Exchange with ^{31}P EXSY NMR Spectroscopy: Synthesis and Characterization of the $[E_7PtH(PPh_3)]^{2-}$ Zintl Ion Complexes [E = P, As]

Banu Kesanli,† Scott Charles,† Yiu-Fai Lam,† Simon G. Bott,‡ James Fettinger,† and Bryan Eichhorn*,†

Contribution from the Department of Chemistry and Biochemistry, University of Maryland, College Park, Maryland 20742, and Department of Chemistry, University of Houston, University Park, Houston, Texas 77204

Received March 20, 2000

Abstract: Ethylenediamine (en) solutions of E_7^{3-} (E = P, As) react with $Pt(PPh_3)_2(C_2H_4)$ in the presence of 4,7,13,16,21,24-hexaoxa-1,10-diazobicyclo[8.8.8]hexacosane (2,2,2-crypt) to give the transition-metal Zintl ion complexes $[P_7PtH(PPh_3)]^{2-}$ (**1**) and $[As_7PtH(PPh_3)]^{2-}$ (**2**) as isomorphic $[K(2,2,2\text{-crypt})]^+$ salts, respectively. The hydride ligand originates from the solvent, and deuterium labeling studies show that the order of hydrogen sources follows the sequence en > CH_3CN > DMSO > DMF in the synthesis of **1**. The $[E_7PtH(PPh_3)]^{2-}$ anions have C_1 point symmetry with unperturbed nortricyclane-like E_7^{3-} ligands bound η^2 to square planar $Pt^{II}H(PPh_3)^+$ centers. Complex **1** is dynamic in solution whereby the $PtH(PPh_3)^+$ fragment shifts from the top to bottom of the P_7 cluster (an $\eta^2 \rightarrow \eta^4 \rightarrow \eta^2$ shift) and spins in the P_4 face in a concerted process to give apparent C_{2v} symmetry. We have shown that ^{31}P EXSY NMR experiments at −78 °C permit the separation of the two processes and show that shifting is ∼20 times faster than spinning ($k_{shift} = 160\ s^{-1}$, $k_{spin} = 8\ s^{-1}$).

Introduction

For the past few decades, variable-temperature one-dimensional NMR spectroscopy has been the technique most frequently used to study dynamic processes in solution.[1,2] In the simplest case, the free energy of activation ($\Delta G^{\ddagger}$) can be extracted from the coalescence temperature in a two-site exchange. Recent developments in band-shape analysis allow for quantitative analysis of rate constants at temperatures below coalescence, provided the rate of exchange is commensurate with the chemical shift time scale of the experiment.[3,4] Exchange processes that are slow on the chemical shift time scale or systems that are difficult to model using band-shape methods (i.e., second-order spin systems) require more sophisticated saturation-transfer techniques for analysis of dynamic behavior.[3,5] However, these 1D methods are essentially limited to two-site exchange systems.

In the past 10 years, two-dimensional exchange spectroscopy (2D EXSY) has become the method of choice to study multisite exchange and dynamic processes with high energy barriers. EXSY NMR techniques allow one to study processes that are slow on the chemical shift time scale and distinguish exchange partners in multistep processes.[3] While EXSY spectra have been used in a qualitative sense for several years, recent advances in software analysis have made EXSY a more quantitative tool. In addition, 2D EXSY spectra have been reported for a variety of nuclei such as ^{13}C,[6] ^{31}P,[3,7,8] ^{119}Sn,[9] and ^{131}Xe[10] to name a few.[3]

Baudler has studied the dynamic behavior of many polyphosphides and their alkylated derivatives[11−14] and showed that ^{31}P EXSY spectra could be used to qualitatively assess the fluxional processes in the P_7^{3-} Zintl ion.[11] The fluxional behavior in P_7^{3-} and other polyphosphides involves multisite exchange and second-order spin systems which make them difficult to study by one-dimensional NMR techniques.[13] Recent studies of amorphous $(Li\cdot glyme)_3P_7$ have shown that the P_7^{3-} cluster undergoes intramolecular exchange faster in the solid state than in solution.[15] The transition-metal Zintl ion complexes can also show multisite fluxional behavior that can also occur by intramolecular multistep exchange mechanisms. The origin of the enhanced fluxionality of the transition-metal Zintl ion complexes often resides in the Zintl ions themselves. The mechanisms of the fluxional processes include facile bond breaking and bond making as well as inversion of configuration at a single phosphorus site.[12,13,16−18] In high-symmetry compounds, the mechanism of exchange is often discernible from

† University of Maryland.
‡ University of Houston.

(1) Sandström, J. *Dynamic NMR Spectroscopy*; Academic Press: New York, 1982; p 78.
(2) *Encyclopedia of Nuclear Magnetic Resonance*; Grant, D. M., Harris, R. K., Eds.; Wiley: Chichester, UK, 1996; Vols. 1−8.
(3) Orrell, K. G. *Annu. Rep. NMR Spectrosc.* **1999**, *37*, 1.
(4) Bain, A. D.; Duns, G. J. *Can. J. Chem.* **1996**, *74*, 819.
(5) Bain, A. D.; Cramer, J. A. *J. Magn. Reson., A* **1993**, *103*, 217.
(6) Farrugia, L. J. *J. Chem. Soc., Dalton Trans.* **1997**, 1783.
(7) Bircher, H.; Bender, B. R.; von Philipsborn, W. *Magn. Reson. Chem.* **1993**, *31*, 293.
(8) Heise, J. D.; Raftery, D.; Breedlove, B. K.; Washington, J.; Kubiak, C. P. *Organometallics* **1998**, *17*, 4461.
(9) Willem *J. Organomet. Chem.* **1995**, *485*, 263.
(10) Brotin, T.; Lesage, A.; Emsley, L.; Collet, A. *J. Am. Chem. Soc.* **2000**, *122*, 1171.
(11) Baudler, M.; Ternberger, H.; Faber, W.; Hahn, J. *Z. Naturforsch.* **1979**, *34B*, 1690.
(12) Baudler, M.; Deriesemeyer, L. *Z. Naturforsch.* **1996**, *B51*, 101.
(13) Baudler, M.; Glinka, K. *Chem. Rev.* **1993**, *93*, 1623.
(14) Baudler, M.; Glinka, K. *Chem. Rev.* **1994**, *94*, 3.
(15) Sen, T.; Poupko, R.; Fleischer, U.; Zimmermann, H.; Luz, Z. *J. Am. Chem. Soc.* **2000**, *122*, 889.
(16) Charles, S.; Bott, S. G.; Rheingold, A. L.; Eichhorn, B. W. *J. Am. Chem. Soc.* **1994**, *116*, 8077.

10.1021/ja000988x CCC: $19.00
Published on Web 10/27/2000

1D variable-temperature ^{31}P NMR studies,[13] but extracting rate data and activation parameters is hampered by second-order spin systems and multisite exchange.

Herein we show that 2D ^{31}P EXSY spectroscopy can be used as a quantitative tool to unravel the complicated multistep exchange process in metalated Zintl ion $[P_7PtH(PPh_3)]^{2-}$ (**1**). The details of the synthesis and characterization of **1** and its arsenic analogue, $[As_7PtH(PPh_3)]^{2-}$ (**2**), are also described. A preliminary communication of the $[P_7PtH(PPh_3)]^{2-}$ structure has been reported.[18]

Experimental Section

General Data. All reactions were performed under nitrogen atmosphere in a drybox (Vacuum Atmospheres Co.). General operating procedures in our laboratories have been described elsewhere.[16] ^{1}H and ^{31}P{^{1}H} NMR, ^{31}P 2D EXSY NMR, and ^{31}P VT NMR spectra were recorded on a Bruker DRX500 AVANCE spectrometer. The spectrometer was run locked for ^{1}H and ^{31}P NMR data collections using DMF-d_7/tol-d_8 mixtures as an internal reference for low-temperature studies. ^{31}P{sel-^{31}P} (^{1}H broad band decoupled) homonuclear decoupling NMR experiments were carried out by combining two ^{31}P RF pulses with a Mini-Circuits Inc. directional coupler.

^{31}P{^{1}H} EXSY spectra were recorded at −78 °C with a pulse sequence from the Bruker pulse library NOESYTP, 90°−t_1−90°−t_m−90°−acqu, modified to have ^{1}H broad band decoupled in the phase-sensitive TPPI (time proportion phase increment) mode. A total of 128 scans per FID of 2K data points were used per time increment. A total of 425 time increments were collected. Recycle times were 1 s, which was 5−6 times the measured T1 values. Typical measurement times were 16 h. The resolutions of the FIDs were 25 and 118 Hz/pt in T2 and T1 domains of the raw data sets, respectively. The EXSY measurements were repeated with a series of mixing times, $t_m = 5$ μs, 0.5 ms, 2 ms, 10 ms, 50 ms, 75 ms, and 100 ms.

The forward linear prediction mode from Bruker XWINNMR software version 2.1 was used to process the data, yielding the final 2D matrix of 2K by 1K. The same software was used to determine the diagonal and cross-peak volumes. Cross-peaks were normalized according to the procedure reported by Ramachandran et al.[19] The equilibrium magnetization, $\mathbf{M}_j^0$, necessary for the calculation of rate constants was determined by acquiring the 2D EXSY spectrum with mixing time equal to zero, since $\mathbf{I}_{ij}(0) = \mathbf{M}_j^0$.

The slopes of the buildup curves at $t_m = 0$ were determined by linear regression analysis by using the software KaleidaGraph, version 3.0.4. The matrix calculations were performed numerically by using the software package Mathcad, version 7.0.

Electrospray mass spectra were recorded from DMF solutions on a Finnigan-type mass spectrometer through direct injection. The samples were ionized by using an ESI probe and detected in the negative ion mode. Elemental analyses were performed under inert atmospheres by Desert Analytics, Tucson, AZ, and Atlantic Microlab, Inc., Norcross, GA.

Chemicals. Melts of nominal composition K_3E_7 (E = P, As) were prepared by high-temperature fusion (~1000 °C) of stoichiometric ratios of the elements. The chemicals were sealed in evacuated, silica tubes and carefully heated with a natural gas/oxygen flame. *Caution: Alkali-metal polyphosphorus compounds are known to spontaneously detonate even under rigorously anaerobic conditions. Therefore, these compounds should only be prepared in small quantities (<0.5 g) and should be handled with caution*. 4,7,13,16,21,24-Hexaoxa-1,10-diazobicyclo-[8.8.8]hexacosane (2,2,2-crypt) was purchased from Aldrich. $Pt(PPh_3)_3$, $Pt(PPh_3)_4$, and $Pt(PPh_3)_2(C_2H_4)$ were purchased from Strem and used without further purification. Anhydrous ethylenediamine (en) and DMF were purchased from Fisher, distilled over calcium hydride, vacuum distilled from K_4Sn_9, and stored under nitrogen. DMF-d_7, DMSO-d_6, and Tol-d_8 were purchased from Cambridge Isotopes and used as received.

Synthesis. ***Preparation of [K(2,2,2-crypt)]$_2$[P$_7$PtH(PPh$_3$)].*** A modification of the published procedure[18] was used for the synthesis of this complex. In a drybox, K_3P_7 (30 mg, 0.089 mmol), $Pt(PPh_3)_3$ (88 mg, 0.089 mmol), and 2,2,2-crypt (100 mg, 0.26 mmol) were dissolved in ca. 3 mL of en in a vial. The reaction mixture was stirred for 12 h, producing a dark red solution with a brown precipitate. The reaction mixture was heated gently (~45 °C) to dissolve the precipitate. The resulting dark red, clear solution was immediately filtered through tightly packed glass wool in a pipet. Dark red crystals formed in the reaction vessel after 2 days (88 mg, 59%). ^{31}P{^{1}H} NMR (DMF-d_7, 25 °C): δ (ppm) 24 (PPh_3, pentet, $^1J_{P-P} = 2720$ Hz, $^2J_{P-P} = 8$ Hz), −39 (1P, second-order multiplet), −51 (2P, second-order multiplet), −120 (4P, br). ^{1}H NMR (25 °C): δ (ppm) −10.1 (multiplet, $^1J_{Pt-H} = 1080$ Hz, $^2J_{P-H} \approx 14$ Hz). For labeling studies, $[P_7PtD(PPh_3)]^{2-}$ was prepared as above but using either DMSO-d_6 or DMF-d_7 as the solvent. IR (KBr pellet): ν(Pt−H) (cm^{-1}) 1945, 1881. Anal. Calcd for $C_{56}H_{96}N_6O_{12}K_2P_8Pt$: C, 42.94; H, 6.18; N, 5.37; P, 15.82. Found: C, 42.11; H, 5.90; N, 4.81; P, 16.13. The calculated formula contains one en solvate molecule.

Identical procedures were used to make the title compound from $Pt(PPh_3)_4$ and $Pt(PPh_3)_2(C_2H_4)$ precursors.

Preparation of [K(2,2,2-crypt)]$_2$[As$_7$PtH(PPh$_3$)]. In vial 1, 57 mg (0.089 mmol) of K_3As_7 and 100 mg (0.26 mmol) of 2,2,2-crypt were dissolved in 3 mL of en. In vial 2, 66 mg (0.089 mmol) of $Pt(PPh_3)_2C_2H_4$ was dissolved in 1 mL of toluene, generating a slurry of partially dissolved complex. The contents of vial 2 were added to vial 1, resulting in a dark red solution. The reaction mixture was stirred for 1 h. The solution was concentrated in vacuo to 2 mL and filtered through tightly packed glass wool in a pipet. Small red crystals formed in the reaction vessel after 2 days (25 mg, 16%). ^{31}P NMR (DMSO-d_6, 25 °C): δ (ppm) 26.7 (PPh_3, singlet with ^{195}Pt satellites, $^1J_{Pt-P} = 2770$ Hz). ^{1}H NMR (25 °C): δ (ppm) −10.8 ($^1J_{Pt-H} = 1080$ Hz, $^2J_{P-H} = 17.6$ Hz). IR (KBr pellet): ν(Pt−H) (cm^{-1}) 1951, 1887. Anal. Calcd for $C_{63}H_{104}N_6O_{12}K_2As_7PPt$: C, 38.45; H, 5.30; N, 4.24. Found: C, 38.50; H, 5.22; N, 3.69. The calculated formula contains one en and one toluene solvate molecule per formula unit.

Crystallography. *[K(2,2,2-crypt)]$_2$[P$_7$PtH(PPh$_3$)]*. A dark red block with crystal dimensions 0.11 × 0.14 × 0.17 mm was mounted on a glass fiber in a random orientation. Data collection was performed at 25 °C with Mo Kα radiation ($\lambda = 0.710\,73$ Å) on an Enraf-Nonius CAD-4F diffractometer. Data were collected by using an ω−2θ scan mode with a variable scan rate (0.67−8 deg/min). Periodic monitoring of three check reflections throughout data collection showed less than 1% decay. An empirical absorption correction (DIFABS) and Lorentz and polarization corrections were applied.

The data were indexed on an orthorhombic cell, and the systematic absences indicated space group $P2_12_12_1$. The initial structure was determined from a Patterson map, and the remaining atoms were located by successive least-squares refinements and difference Fourier syntheses. The hydrogen atoms were placed in idealized positions. The structure was successfully refined (MOLEN, Enraf-Nonius) using full-matrix least-squares with the phosphorus, platinum, and potassium atoms anisotropic in the final cycles. All carbon atoms were refined isotropically, and one of the cryptands showed multisite disorder. The highest peak in the final difference map was 1.33 e/Å^3, which was located near Pt.

[K(2,2,2-crypt)]$_2$[As$_7$PtH(PPh$_3$)]. A dark red crystal with approximate dimensions 0.20 × 0.20 × 0.20 mm was placed on the Enraf-Nonius CAD-4 diffractometer. Data were collected [Mo Kα] with ω−2θ scans over the θ range 2.02−19.94°. A total of 3660 unique reflections were collected. Minor variations in intensity were observed (1−3%), and data were not corrected. Four ψ scan reflections were collected over the range 7.8−10.3°, and the absorption correction was applied with transmission factors ranging from 0.6347 to 0.9893, the average being 0.8364. Data were corrected for Lorentz and polarization factors and reduced to F_o^2 and $\sigma(F_o^2)$.

The systematic absences clearly indicated the orthorhombic space group $P2_12_12_1$ (no. 19), which was confirmed by successful solution

(17) Charles, S.; Danis, J. A.; Eichhorn, B. W.; Fettinger, J. C. *Inorg. Chem.* **1997**, *36*, 3772.

(18) Charles, S.; Eichhorn, B. W.; Bott, S. G.; Fettinger, J. C. *J. Am. Chem. Soc.* **1996**, *118*, 4713.

(19) Ramachandran, R.; Knight, C. T. G.; Kirkpatrick, R. J.; Oldfield, E. *J. Magn. Reson.* **1985**, *65*, 136.

and refinement of the structure. The structure was determined by direct methods using the program SHELXS-86 (Pt and seven As atoms) and refined with SHELXL.[20] Hydrogen atoms were placed in calculated positions. All of the non-hydrogen atoms were refined anisotropically, and the structure was refined to convergence. A final difference Fourier map possessed three peaks (~0.953 e/Å^3) within 1.2 Å of the Pt and As atoms.

Results and Discussion

Zerovalent triphenylphosphine platinum complexes $Pt(PPh_3)_4$, $Pt(PPh_3)_3$, and $Pt(PPh_3)_2(C_2H_4)$ react with the E_7^{3-} Zintl ions (E = P, As) in polar aprotic solvents (en, DMF, DMSO, CH_3CN) in the presence of 2,2,2-crypt to give the $[E_7PtH(PPh_3)]^{2-}$ ions where E = P (**1**) or As (**2**) according to eq 1.

$$K_3E_7 + Pt(PPh_3)_2L_n + solv(H_m) + 2(2,2,2\text{-crypt}) \rightarrow [K(2,2,2\text{-crypt})]_2[E_7PtH(PPh_3)] + PPh_3 + L_n + K^+ + solv(H_{m-1})^- \quad (1)$$

$$E = P, As;\ L_n = PPh_3, 2PPh_3, C_2H_4 + PPh_3;\ solv(H_m) = en, DMF, DMSO, CH_3CN$$

The hydride ligands originate from the solvent (see below). The complexes precipitate from en solutions as dark red crystals of the $[K(2,2,2\text{-crypt})]^+$ salts in moderate yields (40−60%). ^{31}P NMR spectroscopic analysis of the crude reaction mixtures indicates that the reactions are virtually quantitative. The salts and their solutions are air and moisture sensitive. The complexes have been characterized by ^1H and ^{31}P NMR spectroscopy, IR spectroscopy, negative ion electrospray mass spectrometry (NI-EMS), microanalysis, and single-crystal X-ray diffraction.

The negative ion mass spectrum of **1** shows the protonated molecular ion $[HP_7PtH(PPh_3)]^-$ in which the proton presumably originates from the solvent matrix and is attached to the P_7 cage (cf. $[HP_7W(CO)_3]^{2-}$).[21] The deuteride derivative of **1** also appears as the protonated species $[HP_7PtD(PPh_3)]^-$. Slight discrepancies in the intensities and broadness of the peaks in the deuteride spectrum presumably result from small amounts of the hydride complex in the sample. Attempts to prepare the protonated monoanions in solution were unsuccessful.

In contrast to similar reactions with zerovalent 12-electron organometallic precursors, the putative $[P_7Pt(PPh_3)]^{3-}$ is apparently unstable and activates solvent in a formal oxidative addition process to form **1**. The formation of **1** has been monitored at low temperatures (−78 °C, DMF-d_7/tol-d_8 mixture) by using ^{31}P NMR spectroscopy. At short reaction times, only the starting materials, P_7^{3-} and $Pt(PPh_3)_2L_n$, and free PPh_3 are observed in solution. At longer reaction times (~1 h, −78 °C), the resonances for **1** grow in but no intermediates are observed. The absence of a $[P_7Pt(PPh_3)]^{3-}$ intermediate contrasts the chemistry of the $Ni(CO)_2(PPh_3)_2$ that gives the $[P_7Ni(CO)]^{3-}$ as a stable complex (eq 2).

$$P_7^{3-} + Ni(CO)_2(PPh_3)_2 \rightarrow [\eta^4\text{-}P_7Ni(CO)]^{3-} + CO + 2\ PPh_3 \quad (2)$$

Although the formation of **1** appears to be a simple protonation of a $[P_7Pt(PPh_3)]^{3-}$ intermediate, the mechanism is clearly more complicated. Various combinations of solvents (deuterated and nondeuterated) were used in eq 1 chemistry, and a summary of the results is given in Table 1. The products were assayed by using both ^1H NMR and NI-EMS to determine whether hydride (Pt−H) or deuteride (Pt−D) products were formed. The competition experiments give rise to the following order of hydride sources: en > CH_3CN > DMSO > DMF.

Table 1. Summary of Deuterium Labeling Studies from Different Solvent Mixtures

solvent mixture[a]	product[b]	solvent mixture[a]	product[b]
en	Pt−H	en/CH_3CN-d_3	Pt−H
DMF-d_7	Pt−D	DMF/CH_3CN-d_3	Pt−D
DMSO-d_6	Pt−D	en/THF-d_8	Pt−H
CH_3CN-d_3	Pt−D	DMF/THF-d_8	Pt−H
en/DMF-d_7	Pt−H	THF/CH_3CN-d_3	Pt−D
en/DMSO-d_6	Pt−H	THF	NR[c]
DMF/DMSO-d_6	Pt−D	NEt_3	NR

[a] pK_a values in DMSO solutions (pK_{DMSO}) are (en) ~36, (DMSO) 35, (THF) >40, and (CH_3CN) 31.3. Data from ref 43. pK_a values for DMF are not available to our knowledge but probably exceed 35. [b] Pt−H = $[P_7PtH(PPh_3)]^{2-}$; Pt−D = $[P_7PtD(PPh_3)]^{2-}$.

Table 2. Summary of Crystallographic Data for $[K(2,2,2\text{-crypt})]_2[P_7PtH(PPh_3)]$ and $[K(2,2,2\text{-crypt})]_2[As_7PtH(PPh_3)]$[a]

	A	B
empirical formula	$C_{54}H_{87}N_4O_{12}P_8PtK_2$	$C_{54}H_{87}As_7K_2N_4O_{12}PPt$
formula weight	1505.40	1812.98
temperature (K)	293(2)	293(2)
wavelength (Å)	0.709 30	0.709 30
crystal system	orthorhombic	orthorhombic
space group	$P2_12_12_1$	$P2_12_12_1$
unit cell dimensions (Å)	a = 17.088(1)	a = 17.303(2)
	b = 19.900(1)	b = 20.1199(14)
	c = 20.030(2)	c = 20.161(2)
volume (Å^3)	6811(1)	7018.7(12)
Z	4	4
density (g/cm^3)	1.468	1.716
abs coeff (mm^{-1})	2.443	5.471
no. of data/restraints/ params	3144/0/380	3660/0/375
final R indices $[I > 2\sigma(I)]$[b]	R1 = 0.0817	R1 = 0.0913
	wR2 = 0.0988	wR2 = 0.1975
largest diff peak (e/Å^3)	1.33	1.604

[a] A = $[K(2,2,2\text{-crypt})]_2[P_7PtH(PPh_3)]$; **B** = $[K(2,2,2\text{-crypt})]_2[As_7PtH(PPh_3)]$. [b] $R1 = \Sigma|F_o - F_c|/\Sigma F_o$; $wR2 = (\Sigma w|(F_o)^2 - (F_c)^2|^2/\Sigma wF_o^2)^{1/2}$.

Structural Studies. The $[K(2,2,2\text{-crypt})]^+$ salts of **1** and **2** are isomorphic, space group $P2_12_12_1$, and have been characterized by single-crystal X-ray diffraction. A summary of the crystallographic data is given in Table 2, and a listing of selected bond distances and angles for both ions is given in Table 3. An ORTEP drawing of **2** is shown in Figure 1. The structure of **1** is virtually identical to that of **2** (see below) and has been previously communicated.[18] For comparison, a common numbering scheme has been used for both compounds.

The ions have C_1 point symmetry with unperturbed E_7 clusters bound η^2 to $[PtH(PPh_3)]$ metal centers. The hydride and PPh_3 ligands are cis to one another in the square planar array. The E(6) and E(7) atoms of the E_7 cages are trans to the hydride and PPh_3 ligands, respectively, and complete the square planar coordination sphere. For electron counting purposes, the complexes can be viewed as η^2-E_7^{3-} ligands bound to 12-electron $PtH(PPh_3)^+$ fragments. In this charge-separated model, each of the metal-bound pnictides in the E_7 cages donate 2 electrons to give 16-electron square planar Pt(II) complexes.

The Pt−PPh_3 bond distances in **1** and **2** are equivalent at 2.22(2) Å (av). The hydride ligands were not located crystallographically but were evident from the ^1H NMR spectra (for **1**, δ(Pt−H) = −10.1 ppm, multiplet, $^1J_{^{195}Pt-^1H}$ = 1080 Hz, $^2J_{^{31}P-^1H} \approx 14$ Hz; for **2**, δ(Pt−H) = −10.8 ppm, doublet,

(20) Sheldrick, G. *Acta Crystallogr.* **1990**, *A46*, 467.
(21) Charles, S.; Danis, J. A.; Mattamana, S. P.; Eichhorn, B. W.; Fettinger, J. C. *Z. Anorg. Allg. Chem.* **1998**, *624*, 823.

Table 3. Selected Bond Lengths (Å) and Angles (deg) for $[K(2,2,2\text{-crypt})]_2[P_7PtH(PPh_3)]$ and $[K(2,2,2\text{-crypt})]_2[As_7PtH(PPh_3)]$

	1 (E = P)	**2** (E = As)		**1** (E = P)	**2** (E = As)
Pt(1)−P(8)	2.23(1)	2.211(12)	E(3)−E(7)	2.15(2)	2.414(6)
Pt(1)−E(7)	2.40(1)	2.499(4)	E(4)−E(6)	2.14(2)	2.403(7)
Pt(1)−E(6)	2.42(1)	2.509(5)	E(4)−E(5)	2.26(2)	2.459(7)
E(1)−E(2)	2.16(2)	2.347(7)	E(5)−E(7)	2.16(2)	2.403(6)
E(1)−E(3)	2.15(2)	2.347(7)	P(1)−C(11)	1.80(4)	1.81(4)
E(2)−E(4)	2.22(2)	2.437(7)	P(1)−C(31)	1.88(4)	1.83(4)
E(2)−E(5)	2.26(2)	2.480(7)	P(1)−C(21)	1.81(4)	1.91(4)
E(3)−E(6)	2.18(2)	2.403(7)			
P(8)−Pt(1)−E(7)	174.5(4)	174.9(3)	E(6)−E(4)−E(5)	101.6(6)	100.7(2)
P(8)−Pt(1)−E(6)	98.6(4)	94.6(3)	E(2)−E(4)−E(5)	60.6(6)	60.9(2)
E(7)−Pt(1)−E(6)	78.2(4)	83.3(2)	E(7)−E(5)−E(4)	99.3(6)	100.2(2)
E(2)−E(1)−E(3)	97.3(6)	99.0(2)	E(7)−E(5)−E(2)	104.1(7)	104.9(2)
E(1)−E(2)−E(4)	107.7(8)	108.5(3)	E(4)−E(5)−E(2)	58.9(5)	59.1(2)
E(1)−E(2)−E(5)	108.5(7)	107.7(2)	E(3)−E(6)−E(4)	101.0(7)	100.7(2)
E(4)−E(2)−E(5)	60.5(5)	60.0(2)	E(3)−E(6)−Pt(1)	87.9(5)	88.2(2)
E(1)−E(3)−E(6)	104.4(6)	106.0(3)	E(4)−E(6)−Pt(1)	93.0(5)	91.3(2)
E(1)−E(3)−E(7)	108.2(7)	106.9(3)	E(5)−E(7)−E(2)	101.9(6)	100.6(2)
E(6)−E(3)−E(7)	89.2(6)	87.4(2)	E(5)−E(7)−Pt(1)	94.1(5)	91.9(2)
E(6)−E(4)−E(2)	104.6(7)	104.5(2)	E(3)−E(7)−Pt(1)	81.1(5)	88.2(2)

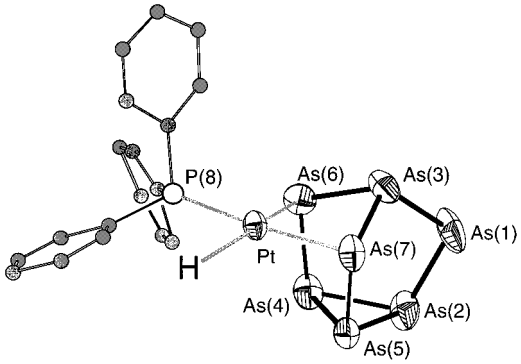

Figure 1. ORTEP drawing of the $[As_7PtH(PPh_3)]^{2-}$ ion.

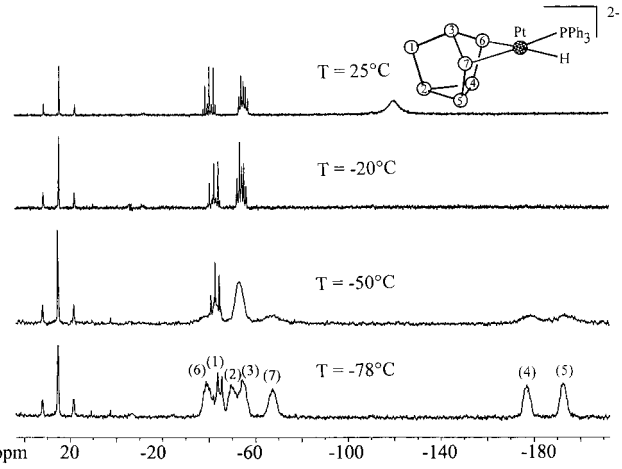

Figure 2. Variable-temperature $^{31}P\{^1H\}$ NMR spectra for $[P_7PtH(PPh_3)]^{2-}$ recorded in DMF-d_7 at 202.4 MHz. The numeric labels on the low-temperature limiting spectrum are peak assignments corresponding to the atom labeling scheme used for the complex.

$^1J_{^{195}Pt-^1H} = 1080$ Hz, $^2J_{^{31}P-^1H} = 18$ Hz). The average Pt−P bond to the P_7 cage in **1** is 2.41(2) Å and is significantly longer than Pt−P bonds involving phosphine ligands (2.2−2.3 Å, av). The Pt−As bonds in **2** (2.50(1) Å, av) are approximately 0.1 Å longer than the Pt−P_7 contacts in **1,** which is consistent with the 0.12 Å increase in the covalent radius of As relative to P.[22] There is an apparent lengthening of the Pt−E(6) bonds in both complexes (the E atom trans to the hydrides) relative to the Pt−E(7) bonds; however, the differences are not statistically relevant. The E(7)−Pt−E(6) angle is more acute in **1** relative to **2** due to the smaller bite angle of the P_7 cage relative to As_7.

The E−E bonds within the E_7 cages are quite similar to those of the unligated E_7^{3-} parent ions. The As−As bonds in **2** are, on average, 0.19−0.25 Å longer than the corresponding P−P bonds in **1**.[22] The heights of the E_7 fragments of the compounds (i.e., the distance from the E(2)−E(4)−E(5) basal planes to the apical E(3) atoms, *h*) are 3.04 and 3.37 Å for **1** and **2**, respectively. These heights are indicative of unperturbed E_7 cages and are consistent with the trends in E−E bonds in related compounds.[23,24] For comparison, the distances from the apical phosphorus atom to the center of the basal triangular plane are elongated by 0.15 Å in the neutral R_3P_7 molecules ($h = 3.15$ Å)[25−28] relative to the parent P_7^{3-} ion ($h = 3.00$ Å).[23,29,30] The height of **2** is equivalent to that of the As_7^{3-} ion in Ba_3As_{14} (*h* = 3.38 Å),[31] and relatively compressed with respect to the neutral R_3As_7 compounds ($h = 3.47$ Å, av).[32]

Spectroscopic Studies. The variable-temperature $^{31}P\{^1H\}$ NMR spectra for **1** are shown in Figure 2. The low-temperature limiting spectrum is consistent with the solid-state structure (C_1 symmetry) showing seven independent ^{31}P multiplets arising from the P_7 cluster and a downfield broad doublet with ^{195}Pt satellites due to the PPh_3 ligand. All resonances can be assigned through combinations of 1D selective decoupling and $^{31}P-^{31}P$ COSY experiments (see below), and the peak labels in Figure

(22) Huheey, J. E.; Keiter, E. A.; Keiter, R. L. Inorganic Chemistry. *Principles of Structure and Reactivity*, 4th ed.; Harper & Row: New York, 1993; p 300.
(23) Korber, N.; von Schnering, H.-G. *J. Chem. Soc., Chem. Commun.* **1995**, 1713.
(24) Mattamana, S. P.; Phomphrai, K.; Fettinger, J. C.; Eichhorn, B. W. *Inorg. Chem.* **1998**, *37*, 6222.
(25) Kovács, I.; Baum, G.; Fritz, G.; Fenske, D.; Wiberg, N.; Schuster, H.; Karaghiosoff, K. *Z. Anorg. Allg. Chem.* **1993**, *619*, 453.
(26) Fritz, G.; Schneider, H.-W. *Z. Anorg. Allg. Chem.* **1990**, *584*, 12.
(27) Fritz, G.; Hoppe, K. D.; Hönle, W.; Weber, D.; Mujica, C.; Manriquez, V.; von Schnering, H. G. *J. Organomet. Chem.* **1983**, *249*, 63.
(28) Mujica, C.; Weber, D.; von Schnering, H. G. *Z. Naturforsch.* **1986**, *B41*, 991.
(29) Dahlmann, W.; von Schnering, H. G. *Naturwissenschaften* **1972**, *59*, 420.
(30) von Schnering, H.-G.; Hönle, W.; Marinquez, V.; Meyer, T.; Mensing, C.; Giering, W. *2nd Int. Conf. Solid State Chem., Collect. Abstr. FV54*; Eindhoven, 1982.
(31) Belin, C. H. E.; Mercier, H.; Bonnet, B.; Bernard, M. *C. R. Acad. Sci.* **1988**, *307*, 549.
(32) Hönle, W.; Wolf, J.; von Schnering, H.-G. *Z. Naturforsch., B* **1988**, *43*, 219.

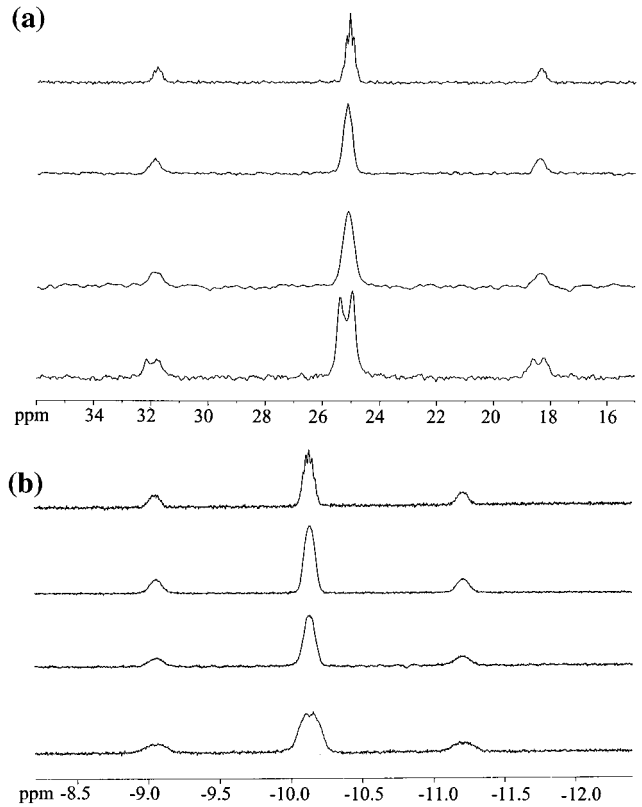

Figure 3. Variable-temperature NMR spectra for $[P_7PtH(PPh_3)]^{2-}$ showing (a, top) the $^{31}P\{^1H\}$ NMR resonance of the PPh_3 ligand and (b, bottom) the ^1H NMR resonance of the hydride ligand. The experimental temperatures are (from bottom to top) −78, −50, −20, and 25 °C for both sets of spectra.

2 correspond to the atom labeling scheme used in Figure 1 and subsequent drawings.

The low-temperature resonances of the hydride and the PPh_3 ligands are convenient starting points for assigning the peaks of the P_7 cage. The variable-temperature ^{31}P NMR spectra for the PPh_3 region and ^1H NMR spectra for the hydride region are shown in parts a and b, respectively, of Figure 3. Both resonances are doublets of multiplets in their limits as is expected due to large couplings from the trans phosphorus atoms in the square planar coordination sphere. Selective decoupling experiments at −78 °C allow for the assignments of the phosphorus atoms trans to these ligands. First, selective ^{31}P-decoupled ^1H NMR experiments, $^1H\{sel\text{-}^{31}P\}$ NMR, show that individually decoupling the ^{31}P resonance at −40.0 ppm results in the collapse of the hydride doublet of multiplets into a single multiplet while individual decoupling of the other six resonances has no appreciable effect. As such the resonance at −40.0 ppm is assigned to P(6) of the P_7 cage. Similarly, $^{31}P\{sel\text{-}^{31}P\}$ NMR experiments show that irradiation of the −67.4 ppm resonance collapses the PPh_3 resonance to a single multiplet whereas irradiation of the other resonances has no effect. Therefore, we can assign the −67.4 ppm resonance to P(7). With these two assignments, the remaining five resonances can be assigned from the −78 °C $^{31}P-^{31}P$ COSY NMR spectrum and are labeled in Figure 2.

Upon warming, the resonances for P(6), P(7), P(4), and P(5) coalesce into the baseline and reemerge above −20 °C as a single resonance of intensity 4 (Figure 2). The resonances for P(2) and P(3) coalesce at −60 °C to give a single peak of intensity 2 at −53.5 ppm. The P(1) resonance is not affected by the exchange process and remains sharp at all temperatures. In addition, the PPh_3 resonance which is a broad doublet at −78 °C becomes a pentet flanked by Pt satellites ($^1J_{^{195}Pt-^{31}P} = 2720$ Hz) at 25 °C (Figure 3a). Similarly, the hydride resonance is transformed from a doublet of multiplets at −78 °C to a single multiplet at 25 °C, which is also flanked by Pt satellites ($^1J_{^{195}Pt-^1H} = 1080$ Hz). These data are consistent with the intramolecular two-step fluxional process outlined in Scheme 1. In this process, the P_7 shifts from an $\eta^2 \rightarrow \eta^4$ coordination mode to generate an 18-electron $[(\eta^4\text{-}P_7)PtH(PPh_3)]^{2-}$ intermediate, $\mathbf{I_1}$. A second $\eta^4 \rightarrow \eta^2$ shift leaves P(5) and P(4) bound to Pt and forms a bond between P(6) and P(7). The shifting process effectively exchanges P(2) with P(3), P(6) with P(4), and P(7) with P(5). This type of $\eta^2 \rightarrow \eta^4 \rightarrow \eta^2$ shift was observed in the reversible reaction of CO with $[\eta^4\text{-}HP_7W(CO)_3]^{2-}$ to give the $[\eta^2\text{-}HP_7W(CO)_4]^{2-}$ ion as outlined in eq 3.

Scheme 1. Mechanism of Exchange for $[P_7PtH(PPh_3)]^{2-}$

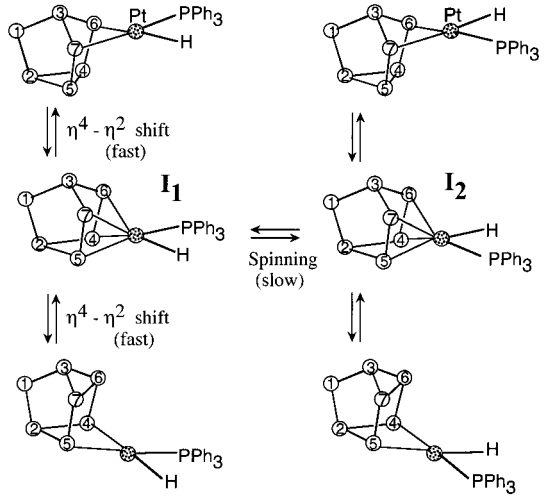

$$[\eta^4\text{-}HP_7W(CO)_3]^{2-} + CO \rightleftharpoons [\eta^2\text{-}HP_7W(CO)_4]^{2-} \quad (3)$$

However, due to the asymmetry in the $PtH(PPh_3)$ group, shifting alone does not exchange all four of the Pt-bound phosphorus atoms. An additional spinning step ($\mathbf{I_1} \rightarrow \mathbf{I_2}$, Scheme 1) is required in the $[(\eta^4\text{-}P_7)PtH(PPh_3)]^{2-}$ intermediate to exchange the four Pt-bound phosphorus atoms. For the isoelectronic $[\eta^4\text{-}P_7W(CO)_3]^{3-}$ ion, spinning of the C_{3v} $W(CO)_3$ fragment attached to the C_{2v} P_7 cluster is rapid on the NMR time scale at −60 °C (80 MHz, DMF-d_7).[16] Because the two processes in Scheme 1 occur simultaneously, determination of the relative rate constants for the two processes (k_{shift} and k_{spin}) is not possible by line shape analysis of the variable-temperature 1D spectra. The broad, second-order nature of the limiting spectra further complicates a potential line shape simulation, and even an average rate constant, k_{obs}, would be difficult to extract by this method.

2D EXSY NMR is a technique which is ideal for studying multisite exchange pathways under equilibrium conditions. The EXSY experiment is similar to a NOESY experiment except cross-peaks are observed between nuclei that are in dynamic chemical exchange.[33] The rate constants associated with the exchange process can be calculated from the cross-peak intensities of the 2D EXSY spectrum without a line shape analysis.

Several approaches for calculating rate constants from eq 4 have been developed.[34] The equation relates the cross-peak intensities ($\mathbf{I}_{ij}$)

(33) Jeener, J.; Meier, B. H.; Bachmann, P.; Ernst, R. R. *J. Chem. Phys.* **1979**, *71*, 4546.

(34) Perrin, C. L.; Dwyer, T. J. *Chem. Rev.* **1990**, *90*, 935.

$$\mathbf{I}_{ij}(t_m) = \mathbf{M}_j^0(e^{-\mathbf{R}t_m})_{ij} \quad (4)$$

at mixing time t_m to the rate matrix $\mathbf{R}$[35,36] and the initial equilibrium magnetization vector $\mathbf{M}_j^0$ of the nuclei in site j. The matrix $\mathbf{R}$ contains the rate constant k_{ji}, which is the first-order rate constant for chemical exchange from site j to site i, and the spin lattice relaxation rates ρ_i and ρ_j (i.e., the T_1 values).

$$\mathbf{R} = \begin{bmatrix} \rho_j & -k_{ij} \\ -k_{ji} & \rho_i \end{bmatrix}$$

Two methods were used in this study for calculating the rate constants. Method A, the initial rate approximation,[37] is based on eq 4 above where, at short mixing time, the exponential simplifies to give eq 5.

$$\mathbf{I}_{ij}(t_m) \approx -t_m\mathbf{R}_{ij}\mathbf{M}_j^0 \approx k_{ji}t_m\mathbf{M}_j^0 \qquad i \neq j \quad (5)$$

In this form, the 2D spectrum can be directly related to the exchange matrix R. The rate constant, k_{ji}, can be determined from the slope of a plot of $\mathbf{I}_{ij}/\mathbf{M}_j^0$ versus t_m. This method allows for the separation of direct cross-peaks (i.e., those in nonsaturated direct chemical exchange), which have a nonzero slope, from the indirect cross-peaks, which have a zero slope. It is necessary to use sufficiently short mixing times to have reliable rate constants because the slopes of the buildup curves change drastically at longer t_m values. The disadvantage of method A is the need for multiple t_m values, which requires considerable spectrometer run time.

The matrix method (method B) for calculating rate constants was first described by Perrin and Gipe[36] and subsequently by Bremer et al.[38] This method consists of diagonalizing the rate matrix $\mathbf{R}$ from all peak volume data at a single t_m. The values of the forward and reverse rate constants can be read from the matrix directly.

The matrix equation is given by eq 6, where $A_{ij} = \mathbf{I}_{ij}(t_m)/\mathbf{M}_j^0$ and $\mathbf{X}$ is the square matrix of eigenvectors of $\mathbf{A}$,

$$R = -\frac{\ln \mathbf{A}}{t_m} = -\frac{\mathbf{X}(\ln \Lambda)\mathbf{X}^{-1}}{t_m} \quad (6)$$

such that $\mathbf{X}^{-1}\mathbf{A}\mathbf{X} = \Lambda = \mathrm{diag}(\lambda_i)$ and $\ln \Lambda = \mathrm{diag}(\ln \lambda_i)$, where λ_i is the ith eigenvalue of $\mathbf{A}$. Although eq 6 looks formidable, it is quite easy to extract the rate constants using commercial software. Experimental intensities are the only input necessary to solve for the eigenvalues and eigenvectors of $\mathbf{A}$ and perform matrix multiplications. Application of this technique to ^{31}P exchange has been described by von Philipsborn,[7] Kubiak,[8] and others.[39,40]

^{31}P EXSY spectra for **1** were recorded at −78 °C in DMF-d_7/tol-d_8 mixtures with mixing times in the range of 5 μs to 100 ms. Spectra with t_m = 10, 50, and 100 ms are shown in Figure 4. To confirm that the observed cross-peaks were due to exchange and not a result of either NOE or J leakage (i.e., unfiltered COSY peaks), the following experiments were performed. First, with t_m = 5 μs (the instrumental limit), chemical exchange is too slow to be detected in the EXSY experiment and only residual COSY peaks should be observed. The EXSY spectrum for **1** with t_m = 5 μs showed no cross-peaks, indicating that J leakage is not occurring in these experiments. Second, a ROESY experiment at −78 °C, which separates NOE and exchange effects, showed no NOE cross-

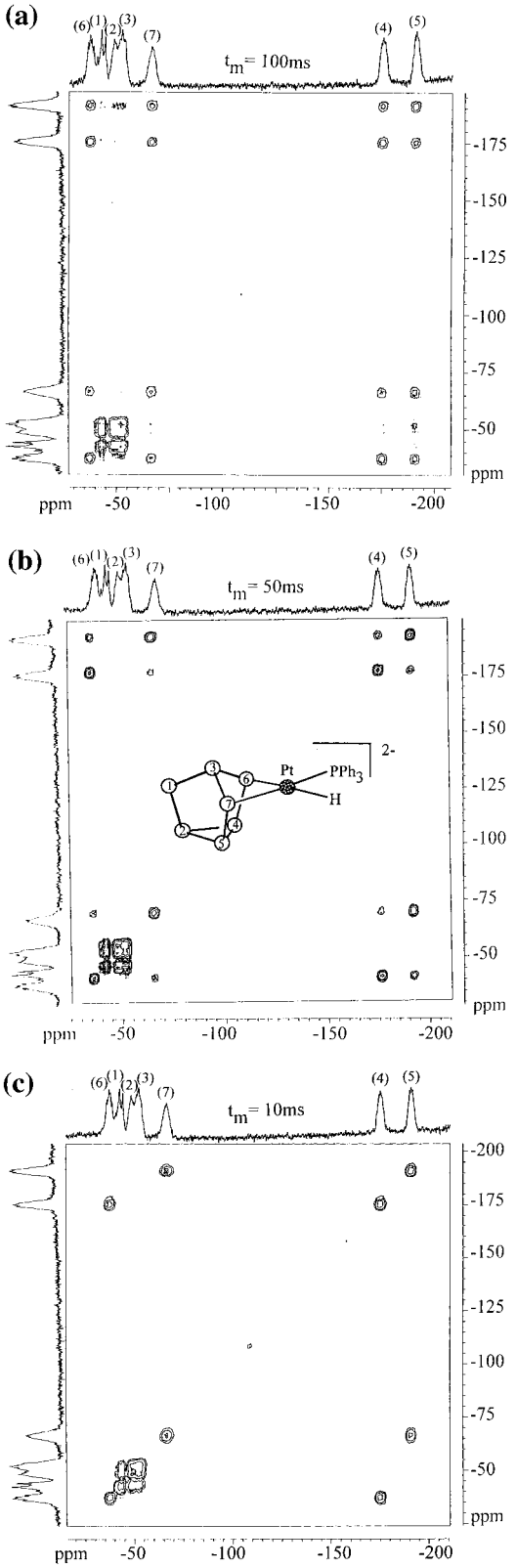

Figure 4. ^{31}P{^{1}H} EXSY NMR spectra for $[P_7PtH(PPh_3)]^{2-}$ recorded at −78 °C, 202.4 MHz, and various mixing times, t_m. The numeric labels on the horizontal spectra correspond to the phosphorus peak assignments.

(35) Macura, S.; Ernst, R. R. *Mol. Phys.* **1980**, *41*, 95.
(36) Perrin, C. L.; Gipe, R. K. *J. Am. Chem. Soc.* **1984**, *106*, 4036.
(37) Kumar, A.; Wagner, G.; Ernst, R. R.; Wuthrich, K. *J. Am. Chem. Soc.* **1981**, *103*, 3654.
(38) Bremer, J.; Mendz, G. L.; Moore, W. J. *J. Am. Chem. Soc.* **1984**, *106*, 4691.
(39) Li, D. W.; Bose, R. N. *J. Chem. Soc., Dalton Trans.* **1994**, 3717.
(40) Malaisselagae, F.; Willem, R.; Penders, M.; Malaisse, W. J. *Mol. Cell. Biochem.* **1992**, *115*, 137.

peaks between P(6)−P(7) and P(4)−P(5) nuclei; however, the large frequency separation between the P(6)−P(4) and P(7)−P(5) pairs of resonances precluded analysis of NOE effects due to dynamic range limitations of the instrument. However, EXSY spectra recorded at −63 °C yielded rate constants ca. 6 times larger than those at −78 °C (see below), which is consistent with cross-peaks due to chemical exchange (a temperature-dependent process) and not NOE (virtually temperature-independent). As such, the EXSY data can be analyzed on the basis of chemical exchange, and other extraneous contributions can be neglected.

Visual inspection of the EXSY spectra in Figure 4 reveals three different exchange situations. At long mixing times (t_m = 100 ms, Figure 4a (top)), spinning and shifting (Scheme 1) are fast on the NMR time scale and equal-intensity cross-peaks are observed for all of the P(4), P(5), P(6), and P(7) pairs. This situation indicates direct and indirect exchange is occurring and the cross-peak intensity is saturated. At shorter mixing times (t_m = 50 ms, Figure 4b (middle)), large exchange cross-peaks are observed between the P(4)−P(6) and P(5)−P(7) pairs of resonances, with the remaining peaks being of diminished intensity. In this regime, the EXSY experiment can separate the different steps, one fast and one slow, in the exchange process outlined in Scheme 1. At shorter mixing times (t_m = 10 ms), only the fast step of the exchange mechanism is detectable, which gives rise to cross-peaks between the P(4)−P(6) and P(5)−P(7) pairs (Figure 4c (bottom)). Qualitatively, these data indicate that the P(4)−P(6) and P(5)−P(7) exchange is fast (the $\eta^2 \rightarrow \eta^4 \rightarrow \eta^2$ shift, Scheme 1) relative to exchange between the P(6)−P(7) and P(4)−P(5) pairs (spinning, Scheme 1). Chemical exchange between the P(6)−P(5) and P(7)−P(4) pairs must occur by indirect means involving a shift + spin process. The rate of this indirect process is governed by the rate-determining step of the shift + spin exchange process, which is the spinning step. Therefore, exchange between P(6)−P(7) and P(4)−P(5) pairs, which occurs through a direct (spinning) process, has the same rate constant as the indirect (spinning + shifting) exchange process involving the P(6)−P(5) and P(7)−P(4) pairs. While we cannot exclude other exchange mechanisms, the data seem most consistent with the process outlined in Scheme 1. An alternative process involving an $\eta^2 \rightarrow \eta^2 \rightarrow \eta^2$ "walk" of the $PtH(PPh_3)$ unit down an edge of the P_7 cage is unlikely. In such a mechanism, the $PtH(PPh_3)$ unit would bridge an edge in the exchange process (e.g., the P(7)−P(5) edge) rather than form the η^4 intermediate (e.g., I_1, Scheme 1). From a P(7)−P(5) edge-bridged η^2 transition state, the probability of the $PtH(PPh_3)$ unit moving to the P(1)−P(7) edge is the same as that for moving back to the P(7)−P(6) edge. Repetition of this process would exchange all phosphorus nuclei in the P_7 cage to generate a single, time-averaged resonance in the fast exchange limit. Since the P(1) resonance does not become involved in the exchange process and the other nuclei exchange in a pairwise fashion, this mechanism is inconsistent with the observed data.

Rate constants were extracted from the EXSY data by using the method of initial rates (method A) and matrix analysis method (method B) described above. A summary of the rate data is given in Table 4. Importantly, the two methods of analysis give the same rate constants within experimental error. In addition, the rate constants show that the $\eta^2 \rightarrow \eta^4 \rightarrow \eta^2$ shift (k_{shift} = 160 s^{-1}, av) is approximately 20 times faster than spinning (k_{spin} = 8 s^{-1}, av). The rate constants at −63 °C are significantly faster ($k_{shift} \approx 10^3$ s^{-1}, av; $k_{spin} \approx 60$ s^{-1}, av), which is again consistent with an all-exchange-type process.

Table 4. Rate Constants[a] for the Dynamic Exchange Process[b] in $[P_7PtH(PPh_3)]^{2-}$

k (s^{-1})	method A	method B	k (s^{-1})	method A	method B
Fast Process (Shifting)[b]					
k_{64}	150	153	k_{75}	137	156
k_{46}	159	176	k_{57}	156	161
Slow Process (Spinning)[b]					
k_{67}	6.8	7.0	k_{45}	7.4	7.9
k_{76}	9.7	8.5	k_{54}	6.2	7.4

[a] Rates determined from volume integration of EXSY off-diagonal peaks. Method A = initial rate approximation method. Method B = matrix analysis method. See the Experimental Section for details. [b] See Scheme 1 for definitions of rate constants and the steps in the exchange mechanism. Data were collected at −78 °C.

Conclusions

von Philipsborn and co-workers first showed that inequivalent $^{31}P-^{31}P$ EXSY NMR peak intensities could be used to identify inter- and intramolecular exchange processes in [Rh(*S,S*-chiraphos)(mac)]$^+$ complexes (mac = α-*N*-acetylcinnamate).[7] The use of $^{31}P-^{31}P$ EXSY NMR spectroscopy in the study of the dynamic behavior of **1** is, to our knowledge, the first example of an intramolecular multistep fluxional process in which the individual steps could be quantitatively separated. In future studies, we shall show that precise kinetic data can be extracted in related dynamic systems where traditional line shape analysis hampered by second-order spin systems limited access to limiting spectra.

The formation of compounds **1** and **2** from zerovalent Pt precursors is an unusual example of metal-based chemistry with transition-metal Zintl ion compounds. Related compounds such as $[\eta^4\text{-}P_7Ni(CO)]^{3-}$, $[\eta^2\text{-}P_7W(CO)_4]^{3-}$, and $[\eta^4\text{-}E_7M(CO)_3]^{3-}$, where E = P, As, and Sb and M = Cr and Mo, all show ligand-based chemistry with protons and other electrophiles (i.e., reactions at the E_7 cluster).[16−18,21,41,42] Pt complexes are of course well-known for C−H activation chemistry, but the trends in C−H activation in eq 1 are unusual. While we do not understand the detailed mechanism of hydride formation at present, the reaction appears to require a coordinating ligand for hydride formation and is not a simple protonation. Spectroscopic studies on the $[E_7M(CO)_3]^{3-}$ ions have shown the E_7^{3-} ligands to be potent electron donors. As such, a zerovalent 16-electron $[\eta^2\text{-}P_7Pt(PPh_3)]^{3-}$ intermediate would be very nucleophilic and prone to oxidative addition chemistry. It is interesting to note that addition of a proton to the P_7 cage leaves the metal in the zerovalent state (e.g., $[\eta^4\text{-}HP_7Ni(CO)]^{2-}$) whereas the present compounds formally contain an oxidized Pt(II) center.

Acknowledgment. We thank the donors of the Petroleum Research Fund and the NSF (Grant CHE 9500686 for support of this work. We are indebted to Dr. Kangyan Du for the NI-EMS data and Dr. Sundeep Mattamana for experimental assistance. We thank Prof. Wolfgang von Philipsborn for very helpful discussions.

Supporting Information Available: Complete listing of crystallographic data for $[K(2,2,2\text{-crypt})]_2[As_7PtH(PPh_3)]$ (PDF). This material is available free of charge via the Internet at http://pubs.acs.org.

JA000988X

(41) Charles, S.; Fettinger, J. C.; Eichhorn, B. W. *J. Am. Chem. Soc.* **1995**, *117*, 5303.
(42) Charles, S.; Eichhorn, B. W.; Fettinger, J. C.; Bott, S. G. *Inorg. Chem.* **1996**, *35*, 1540.
(43) Bordwell, F. G. *Acc. Chem. Res.* **1988**, *21*, 456.